Earth and Planetary Science Letters 454 (2016) 293–303

Contents lists available at ScienceDirect

Earth and Planetary Science Letters

www.elsevier.com/locate/epsl

Molybdenum isotopic evidence for the origin of chondrules and a distinct genetic heritage of carbonaceous and non-carbonaceous meteorites

Gerrit Budde *, Christoph Burkhardt, Gregory A. Brennecka, Mario Fischer-Gödde, Thomas S. Kruijer, Thorsten Kleine

Institut für Planetologie, University of Münster, Wilhelm-Klemm-Straße 10, 48149 Münster, Germany

ARTICLE INFO

Article history:
Received 10 May 2016
Received in revised form 1 September 2016
Accepted 9 September 2016
Available online 3 October 2016
Editor: B. Marty

Keywords:
Mo isotopes
nucleosynthetic anomalies
chondrule formation
complementarity
isotopic dichotomy
gas giants

ABSTRACT

Nucleosynthetic isotope anomalies are powerful tracers to determine the provenance of meteorites and their components, and to identify genetic links between these materials. Here we show that chondrules and matrix separated from the Allende CV3 chondrite have complementary nucleosynthetic Mo isotope anomalies. These anomalies result from the enrichment of a presolar carrier enriched in *s*-process Mo into the matrix, and the corresponding depletion of this carrier in the chondrules. This carrier most likely is a metal and so the uneven distribution of presolar material probably results from metal–silicate fractionation during chondrule formation. The Mo isotope anomalies correlate with those reported for W isotopes on the same samples in an earlier study, suggesting that the isotope variations for both Mo and W are caused by the heterogeneous distribution of the same carrier. The isotopic complementary of chondrules and matrix indicates that both components are genetically linked and formed together from one common reservoir of solar nebula dust. As such, the isotopic data require that most chondrules formed in the solar nebula and are not a product of protoplanetary impacts.

Allende chondrules and matrix together with bulk carbonaceous chondrites and some iron meteorites (groups IID, IIIF, and IVB) show uniform excesses in ^{92}Mo, ^{95}Mo, and ^{97}Mo that result from the addition of supernova material to the solar nebula region in which these carbonaceous meteorites formed. Non-carbonaceous meteorites (enstatite and ordinary chondrites as well as most iron meteorites) do not contain this material, demonstrating that two distinct Mo isotope reservoirs co-existed in the early solar nebula that remained spatially separated for several million years. This separation was most likely achieved through the formation of the gas giants, which cleared the disk between the inner and outer solar system regions parental to the non-carbonaceous and carbonaceous meteorites. The Mo isotope dichotomy of meteorites provides a new means to determine the provenance of meteoritic and planetary materials, and to assess genetic links between chondrites and differentiated meteorites.

1. Introduction

Nucleosynthetic isotope anomalies in meteorites and their components provide unique insights into the formation and early evolution of the solar system (see Dauphas and Schauble, 2016 for an overview). These anomalies arise through the heterogeneous distribution of isotopically diverse presolar materials in the solar protoplanetary disk and as such can be used to assess potential genetic relationships among meteorites and their components. For instance, on the basis of Cr, Ti, and O isotopic data, Warren (2011) distinguished between carbonaceous and non-carbonaceous meteorites and argued that this distinction reflects a fundamental dichotomy in the provenance of meteoritic and planetary materials. This dichotomy may reflect a temporal change in the composition of the solar nebula, perhaps caused by episodic accretion of material to the solar nebula (e.g., Wasson, 2000), or, alternatively, is due to the formation of carbonaceous and non-carbonaceous meteorites in spatially distinct regions of the solar nebula (e.g., Warren, 2011).

Nucleosynthetic isotope anomalies also exist at a smaller scale among the components of primitive meteorites; these isotope anomalies are most prominent in Ca–Al-rich inclusions (CAIs) (e.g., Dauphas and Schauble, 2016), but are also present in chondrules and matrix, the major components of most primitive chon-

* Corresponding author.
E-mail address: gerrit.budde@uni-muenster.de (G. Budde).

http://dx.doi.org/10.1016/j.epsl.2016.09.020

drites. For instance, chondrules and matrix from the Allende carbonaceous chondrite (CV3) have complementary nucleosynthetic W isotope anomalies, indicating that presolar material is unevenly distributed between these two components (Budde et al., 2016). This isotopic complementarity confirms earlier conclusions based on the chemical complementarity of chondrules and matrix (Becker et al., 2015; Bland et al., 2005; Ebel et al., 2016; Hezel and Palme, 2008, 2010; Palme et al., 2015) that both components are genetically linked and formed from the same reservoir of solar nebula dust. As such, these data would rule out the formation of chondrules by protoplanetary impacts and would instead indicate a solar nebula origin of chondrules. However, the heterogeneous distribution of presolar material between chondrules and matrix should lead to collateral isotopic variations for elements other than W. Thus, given the importance of the isotopic chondrule–matrix complementarity for constraining chondrule formation models, it is necessary to identify such anomalies also for other elements. Demonstrating isotopic chondrule–matrix complementarity for several elements, and the absence of such anomalies for some other elements, may also help to better understand the nature of the presolar carrier that is unevenly distributed between chondrules and matrix, as well as the processes leading to this uneven distribution. Such information is critical for better constraining the nature of the chondrule-forming process.

Here we report Mo and Ba isotopic data for the same Allende chondrule and matrix samples analyzed previously for W isotopes (Budde et al., 2016). Molybdenum is particularly useful because it exhibits large and distinctive nucleosynthetic isotope anomalies in bulk meteorites (Burkhardt et al., 2011; Dauphas et al., 2002a). Of note, *r*- and *s*-process variability result in different Mo isotope patterns, making it possible to distinguish, for instance, a deficit in *s*-process from an excess in *r*-process Mo nuclides (Burkhardt et al., 2011). Barium is useful because it can provide additional constraints on the nature of the presolar carrier causing the isotopic anomalies in chondrules and matrix. Because Ba is lithophile while Mo and W are siderophile, the combined isotopic data can help to distinguish between different grain types (e.g., metal versus silicates) as the carrier of the observed isotope anomalies.

Using the new isotopic data, we will assess the extent of isotopic complementarity of chondrules and matrix, evaluate the carrier causing this complementarity and discuss the implications of these constraints for the origin of chondrules. In addition, the Mo isotope data provide new insights into the genetic heritage of distinct meteorite parent bodies and the origin of the dichotomy observed between carbonaceous and non-carbonaceous meteorites, which in turn bears testimony to the early dynamical evolution of the solar nebula and formation of the gas giants.

2. Samples and analytical methods

The chondrule, matrix, and bulk rock samples from the Allende CV3 chondrite analyzed here are the same samples previously analyzed for their Hf–W isotopic compositions (Budde et al., 2016). In total three matrix separates, six chondrule fractions, and two bulk rock samples of Allende were analyzed. The chondrule fractions comprise between 155 and ~3000 chondrules each and differ in grain size (C2 > C3 > C4) and magnetic susceptibility (C3m > C3i > C3n). Details about the preparation of these samples are given in the supplementary material.

All samples (0.3–0.5 g) were digested in closed Savillex® beakers on a hotplate using HF–HNO_3(–$HClO_4$), followed by inverse *aqua regia*. The samples were then passed through a two-stage anion exchange chemistry used for the separation of W in our previous study (Budde et al., 2016). The Mo and Ba analyzed in the present study were separated from column washes collected during the W separation, which was accomplished following slightly modified procedures outlined in Burkhardt et al. (2011, 2014) and Carlson et al. (2007). In short, Mo was collected during the W anion exchange chemistry using 3 M HNO_3, and was then further purified using Eichrom® TRU Resin and HCl and HNO_3. Barium was separated from the matrix using AG50-X8 cation resin and various strengths of HCl, with Ba eluted in 2.5 M HNO_3 (see supplementary material for details).

The Mo isotope measurements were performed on the Thermo Scientific® Neptune *Plus* MC-ICP-MS at the Institut für Planetologie at the University of Münster. The samples were introduced using a Savillex® C-Flow PFA nebulizer connected to a Cetac® Aridus II desolvator. Standard Ni sample and (H) skimmer cones were used and total ion beam intensities of $\sim 1.3 \times 10^{-10}$ A were obtained for a ~100 ppb Mo solution at a ~50 µl/min uptake rate. Each measurement consumed ~100 ng of Mo and consisted of 40 baseline integrations (on-peak zeros) of 8.4 s each, followed by 100 Mo isotope ratio measurements of 8.4 s each. Instrumental mass bias was corrected by internal normalization to $^{98}Mo/^{96}Mo = 1.453173$ using the exponential law. This normalization is preferred because it results in large Mo isotope anomalies and distinctive isotope patterns (Burkhardt et al., 2011). Isobaric interferences of Zr and Ru on Mo masses were corrected by monitoring ^{91}Zr and ^{99}Ru (see supplementary material for details). The Mo isotope data are reported as $\varepsilon^{i}Mo$ values relative to the mean of bracketing runs of the Alfa Aesar® solution standard, where $\varepsilon^{i}Mo = [(^{i}Mo/^{96}Mo)_{sample}/(^{i}Mo/^{96}Mo)_{standard} - 1] \times 10^{4}$. For samples analyzed several times, reported values represent the mean of pooled solution replicates. The accuracy and precision of the Mo isotope measurements were assessed by repeated analyses of the BHVO-2 rock standard (Table S2), several digestions of which were processed through the full analytical protocol and analyzed together with each set of samples. The $\varepsilon^{i}Mo$ values obtained for BHVO-2 are indistinguishable from the Alfa Aesar standard, demonstrating that the Mo isotopic data are accurate. The external reproducibility of the Mo isotope measurements, as determined by repeated measurements of BHVO-2, ranged from ±0.14 for $\varepsilon^{97}Mo$ to ±0.39 for $\varepsilon^{92}Mo$ (2 s.d., $n = 24$). Total procedural blanks were between 0.7 and 1.2 ng and thus negligible, given that several hundred ng of Mo were analyzed for each sample.

The Ba isotope measurements were made on the Thermo Scientific® Triton *Plus* TIMS at the Institut für Planetologie at the University of Münster. Barium was analyzed using zone-refined double Re filaments with Ba loaded directly on the filament in 2 M HCl. Due to the setup of the specific instrument, the alignment of all Ba isotopes and required interference monitors was not possible on a single line and therefore no data is reported for ^{132}Ba. However, all other isotopes of Ba, along with La and Ce, which have direct isobaric interferences with Ba, were monitored during the measurements. Each run consisted of 300–600 ratios with 16 s integration times. ^{134}Ba, ^{135}Ba, ^{136}Ba, ^{137}Ba, ^{138}Ba, and ^{140}Ce were measured during a single static run utilizing 10^{11} Ω resistors; 10^{12} Ω resistors were used to measure ^{130}Ba and ^{139}La. Data are fractionation corrected to $^{134}Ba/^{136}Ba = 0.3078$ using the exponential law (Carlson et al., 2007). The external reproducibility of the Ba isotope measurements was assessed using the long-term reproducibility of terrestrial basalt samples put through the same chemical and measurement procedures as the samples from this study, ranging from ±0.13 for $\varepsilon^{135}Ba$ to ±0.31 for $\varepsilon^{138}Ba$ (2 s.d., $n = 14$). All run data are given in Tables 1 and S4.

3. Results

The Mo concentration and isotope data for the investigated Allende samples are provided in Table 1. Compared to bulk Allende, the matrix samples are enriched in Mo, while the chondrule separates are variably depleted in Mo. The largest variations in Mo

Table 1
Mo, Ba, and W isotope data for matrix, chondrule, and bulk samples of Allende.

Sample	Mo (ng/g)	W[a] (ng/g)	N	ε^{92}Mo (±2σ)	ε^{94}Mo (±2σ)	ε^{95}Mo (±2σ)	ε^{97}Mo (±2σ)	ε^{100}Mo (±2σ)	ε^{183}W[a] (±2σ)	ε^{135}Ba (±2σ)
Bulk Allende										
MS-A	**1416**	**166**	5	**1.41 ± 0.27**	**0.97 ± 0.19**	**0.81 ± 0.05**	**0.40 ± 0.08**	**0.44 ± 0.12**	**0.04 ± 0.04**	**0.27 ± 0.13**
MS-B	1424	173	5	0.47 ± 0.18	0.10 ± 0.17	0.49 ± 0.19	0.20 ± 0.10	0.10 ± 0.14	0.17 ± 0.03	0.27 ± 0.13
Allende matrix										
M1	1453	187	5	−3.12 ± 0.21	−2.74 ± 0.12	−1.25 ± 0.05	−0.75 ± 0.08	−0.97 ± 0.11	−1.51 ± 0.15	0.15 ± 0.13
M2	1602	194	2	−2.56 ± 0.39	−2.08 ± 0.28	−0.95 ± 0.20	−0.56 ± 0.14	−0.94 ± 0.23	−0.73 ± 0.15	0.24 ± 0.13
M3	1780	211	5	−1.52 ± 0.17	−1.43 ± 0.16	−0.49 ± 0.08	−0.30 ± 0.05	−0.50 ± 0.11	−0.98 ± 0.15	0.11 ± 0.13
Mean	**1612**	**197**		**−2.40**	**−2.08**	**−0.90**	**−0.54**	**−0.80**	**−1.07**	**0.17**
Allende chondrules										
C1	1188	102	2	2.30 ± 0.39	1.85 ± 0.28	1.42 ± 0.20	0.76 ± 0.14	0.74 ± 0.23	1.79 ± 0.15	0.20 ± 0.13
C2	973	90	2	4.60 ± 0.39	3.66 ± 0.28	2.49 ± 0.20	1.34 ± 0.14	1.54 ± 0.23	1.41 ± 0.15	0.29 ± 0.13
C3m	1496	110	4	3.62 ± 0.11	2.66 ± 0.07	1.84 ± 0.04	0.91 ± 0.07	1.00 ± 0.08	1.39 ± 0.15	0.18 ± 0.13
C3n	628	71	2	7.53 ± 0.39	6.08 ± 0.28	3.98 ± 0.20	2.10 ± 0.14	2.39 ± 0.23	2.17 ± 0.16	0.30 ± 0.13
C3i	1169	89	4	5.62 ± 0.29	4.25 ± 0.14	2.80 ± 0.13	1.45 ± 0.12	1.68 ± 0.27	2.26 ± 0.15	0.21 ± 0.13
C4	976	82	2	5.31 ± 0.39	4.25 ± 0.28	2.83 ± 0.20	1.53 ± 0.14	1.72 ± 0.23	2.04 ± 0.15	–
C3[b]	1071	88		5.26	4.03	2.68	1.38	1.57	1.94	–
C2–C4[c]	**1032**	**87**		**5.15**	**4.01**	**2.68**	**1.40**	**1.60**	**1.85**	–
Mean	1072	91		4.83	3.79	2.56	1.35	1.51	1.84	0.24

Mo isotope ratios are normalized to $^{98}Mo/^{96}Mo = 1.453173$. Uncertainties reported for measured ε^{i}Mo values represent the external reproducibility (2 s.d.) obtained from repeated analyses of BHVO-2 (Table S2) or the 95% confidence interval (95% CI) for samples with $N > 3$. Most representative values are shown in bold. *N*: number of analyses (Mo-IC). Mo concentrations have an uncertainty of ∼3%. Ba isotope data are normalized to $^{134}Ba/^{136}Ba = 0.3078$ and reported as the parts per 10,000 deviation from terrestrial Ba isotope ratios. Uncertainties for ε^{135}Ba represent the external reproducibility obtained from repeated analyses of terrestrial basalt samples. Complete Ba isotope data set is provided in Table S4.

[a] W data are from Budde et al. (2016).

[b] Weighted average of C3m, C3n, C3i (magnetic separates from the same grain size fraction).

[c] Weighted average of C2, C3m, C3n, C3i, C4 (chondrule fractions obtained from the same piece of Allende).

concentrations exist for the different separates of chondrule fraction C3, where the magnetic fraction C3m has the highest and the non-magnetic fraction C3n the lowest Mo concentration. The weighted mean of C3, calculated by recombining all three separates, has a similar Mo concentration as the other three bulk chondrule separates (C1, C2, C4). The mean Mo concentration of the chondrules of ∼1072 ppb is lower than that of bulk Allende (∼1420 ppb Mo), which again is lower than that of the matrix (∼1612 ppb Mo). The complementary enrichment and depletion of Mo in matrix and chondrules is consistent with the distribution of W between these samples (Becker et al., 2015; Budde et al., 2016) (Fig. S1). Thus, overall the elemental Mo–W systematics are consistent with prior observations that chondrules in CV chondrites are depleted in siderophile elements, while the matrix is enriched in these elements (e.g., Palme et al., 2014b).

All analyzed chondrule and matrix samples display well-resolved Mo isotope anomalies, the magnitude of which decrease in the order $\varepsilon^{92}Mo > \varepsilon^{94}Mo > \varepsilon^{95}Mo > \varepsilon^{100}Mo > \varepsilon^{97}Mo$. The chondrule separates all have positive ε^{i}Mo values, while the matrix samples display negative ε^{i}Mo values (Fig. 1). Hence, chondrules and matrix exhibit complementary Mo isotope anomalies. The chondrule fractions show a larger range of Mo isotope anomalies than the matrix and, as for the Mo concentrations, this range is largely defined by the different separates of chondrule fraction C3. The Mo isotope anomalies increase with decreasing magnetic susceptibility of the chondrule fractions from $\varepsilon^{92}Mo \approx 3.6$ for the magnetic fraction C3m to $\varepsilon^{92}Mo \approx 7.5$ for the non-magnetic fraction C3n.

The two analyzed samples of bulk Allende yield significantly different Mo isotope compositions (Figs. 1 and S2); while MS-A shows resolved anomalies, the Mo isotope composition of the MS-B powder is nearly indistinguishable from that of the Alfa Aesar standard and only for ε^{95}Mo shows a resolved anomaly. These results demonstrate significant Mo isotope heterogeneity among bulk samples of Allende, even for samples prepared from powders of ∼40 g and ∼100 g material. This heterogeneity is most likely caused by the uneven distribution of CAIs with highly anomalous

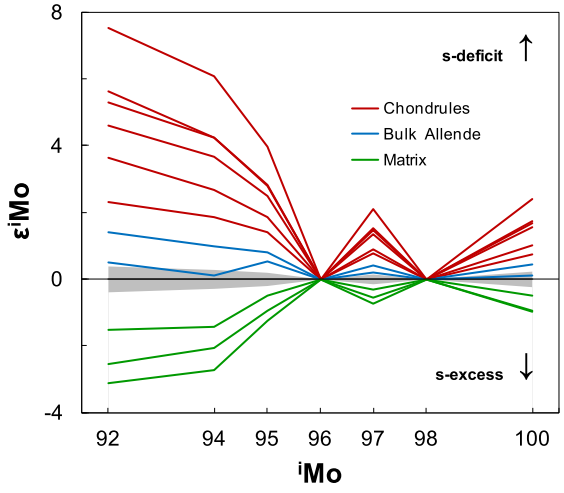

Fig. 1. Mo isotope patterns of the Allende samples. Chondrule fractions (red) show an *s*-deficit, while the matrix (green) has a complementary *s*-excess. The gray area represents the external reproducibility (2 s.d.) of the Mo isotope measurements, defined by repeated analyses of BHVO-2 (Table S2). (For interpretation of the references to color in this figure legend, the reader is referred to the web version of this article.)

Mo isotope compositions such as CAI 'A-ZH-5', which is characterized by $\varepsilon^{92}Mo \approx 22$ (Burkhardt et al., 2011). The large range of Mo isotope compositions for Allende reported here and in previous studies highlights that the true bulk composition of Allende (and possibly other carbonaceous chondrites) is difficult to determine (see supplementary material for details).

In spite of the large Mo isotope anomalies in chondrules, matrix, and bulk samples of Allende, no significant Ba isotope variations are found among these samples (Tables 1 and S4). All chondrule, matrix, and bulk samples exhibit a uniform ε^{135}Ba excess of 0.22 ± 0.12 (2 s.d.), consistent with the results of prior studies (e.g., Bermingham et al., 2016).

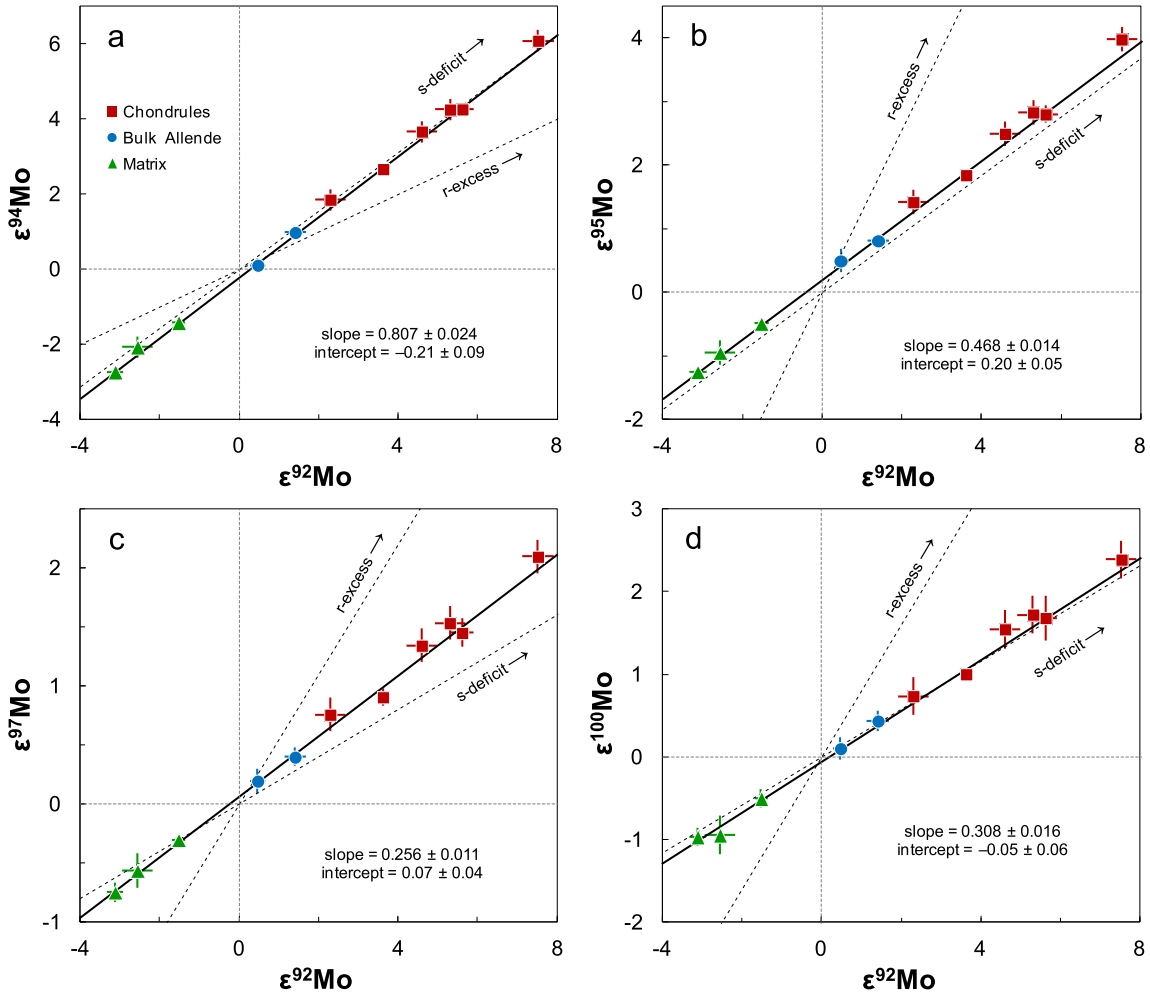

Fig. 2. Plots of ε^{i}Mo versus ε^{92}Mo for the Allende samples. Dashed lines are mixing lines between terrestrial Mo and *s*- or *r*-process Mo, calculated using the *s*-process composition as measured in mainstream SiC grains (Nicolussi et al., 1998) and corresponding *r*-process residuals. Solid lines indicate the regressions calculated by *Isoplot* for the chondrule and matrix samples (note that bulk Allende was *not* included in these regressions). Uncertainties on the slopes and intercepts are 95% confidence levels.

4. Isotopic complementarity of chondrules and matrix and the origin of chondrules

4.1. Heterogeneous distribution of s-process Mo between chondrules and matrix

All chondrule fractions show positive Mo isotope anomalies and the characteristic *w*-shaped Mo isotope pattern indicative of a deficit in *s*-process Mo nuclides (Burkhardt et al., 2011; Dauphas et al., 2002a). In contrast, the matrix separates show negative anomalies and the *m*-shaped Mo isotope pattern characteristic for an excess in *s*-process Mo nuclides. Thus, the Mo isotope data indicate the complementary enrichment and depletion of *s*-process Mo in matrix and chondrules. The heterogeneous distribution of *r*-process nuclides, in contrast, would have resulted in different Mo isotope patterns, which would be characterized by an extra 'kink' at ^{94}Mo. This kink has been observed in coarse-grained type B CAIs (Brennecka et al., 2013; Burkhardt et al., 2011) and is also present in the Mo isotope patterns obtained for some bulk samples of Allende (e.g., MS-B). However, both chondrules and matrix do not show this kink and their Mo isotope patterns are fully consistent with those expected for the uneven distribution of *s*-process matter (Fig. 1).

To assess the nature of the Mo isotope anomalies in more detail, it is useful to plot the data in diagrams of ε^{i}Mo versus ε^{92}Mo. In these diagrams, the chondrule and matrix separates (as well as the bulk Allende samples) plot on single, well-defined correlation lines (Fig. 2). The slopes of these lines are fully consistent with the slopes defined by Mo isotopic data for acid leachates from the Murchison (CM2) and Orgueil (CI1) carbonaceous chondrites (Burkhardt et al., 2012; Dauphas et al., 2002b) (Fig. S3), with those obtained for a mixing line between terrestrial Mo and *s*-process Mo as measured in mainstream SiC grains (Nicolussi et al., 1998), as well as with the slopes predicted by theoretical models of *s*-process nucleosynthesis (e.g., Arlandini et al., 1999). Only for ^{97}Mo, the slopes of the chondrule–matrix and leachate data slightly deviate from that of the calculated *s*-mixing line. Thus, overall the Mo isotopic anomalies in chondrules and matrix are consistent with the expected variations for a heterogeneous distribution of *s*-process matter, where the matrix exhibits an *s*-excess, while chondrules have a complementary *s*-deficit. If instead the Mo isotope variations would be caused by the uneven distribution of *r*-process matter, then both chondrules and matrix should exhibit larger ε^{95}Mo, ε^{97}Mo and ε^{100}Mo anomalies and smaller ε^{94}Mo anomalies (at a given ε^{92}Mo) than observed (Fig. 2).

Since all chondrules and matrix samples plot on single, well-defined ε^{i}Mo–ε^{92}Mo correlation lines (Fig. 2), the Mo isotope variations among them can be attributed to the enrichment of a single presolar carrier of *s*-process Mo in the matrix combined with the complementary depletion of this carrier in the chondrules. In addition, the different chondrule separates themselves also display variable *s*-deficits. Given that each of the chondrule separates con-

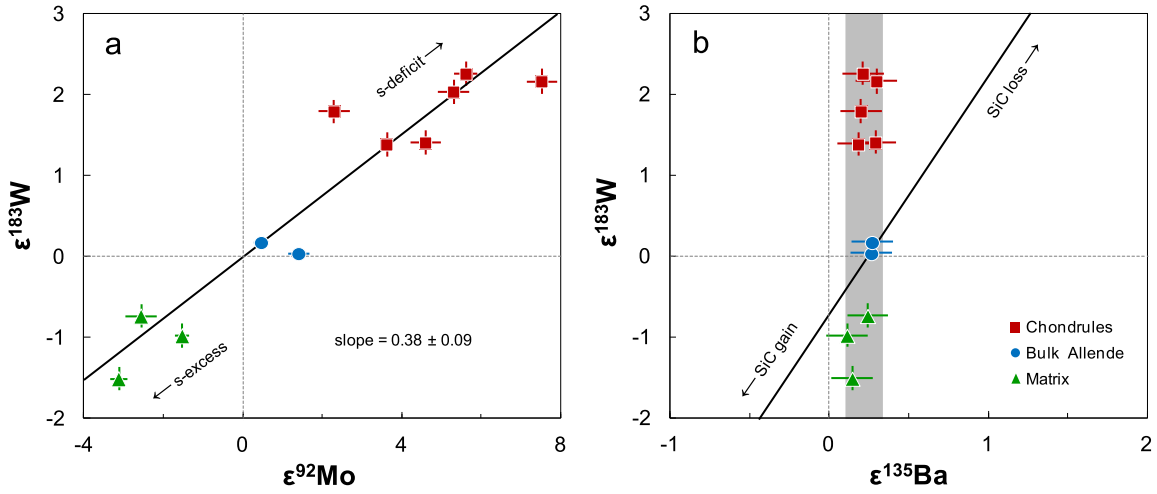

Fig. 3. (a) Plot of ε^{183}W versus ε^{92}Mo for the Allende samples. Solid line indicates the regression through the chondrule and matrix samples. Note, however, that the different chondrule, matrix, and bulk samples of Allende have different W/Mo and are, therefore, not expected to plot on a single mixing line. (b) Plot of ε^{183}W versus ε^{135}Ba for the Allende samples. The solid line is a mixing line between the bulk chondrite and presolar SiC grains. Ba and W isotope compositions in SiC are from Prombo et al. (1993) and Ávila et al. (2012). For the calculation, Ba and W concentrations of 2 and 1.9 ppm in SiC (Ávila et al., 2012, 2013) and CI-chondritic Ba and W concentrations of 2.42 and 0.096 ppm (Palme et al., 2014a) were used. The calculations show that the heterogeneous distribution of SiC between chondrules and matrix would result in correlated W and Ba isotope variations, which is not observed. Note that the SiC Ba concentration used is at the lower range of reported values, whereas the W concentration is an upper limit. Thus, at a given ^{183}W anomaly, the true Ba isotopic anomaly caused by the heterogeneous distribution of SiC, would probably be larger than the calculated anomaly. The grey bar indicates the average and 2 s.d. ($\varepsilon^{135}\text{Ba} = 0.22 \pm 0.12$) of all investigated samples.

sists of a large number of chondrules, the Mo isotope variability among the chondrule separates indicates that there must be even larger Mo isotope variations among individual chondrules. Thus, evidently the carrier of *s*-process Mo responsible for the different Mo isotope compositions of chondrules and matrix is also heterogeneously distributed among the chondrules themselves.

4.2. Carrier of *s*-process anomalies in chondrules and matrix

The nucleosynthetic Mo isotope anomalies of the chondrule and matrix fractions are correlated with those determined for W on the same samples (Budde et al., 2016), and the observed ε^{183}W and ε^{92}Mo variations are consistent with the uneven distribution of *s*-process material (Fig. 3a). Thus, the nucleosynthetic Mo and W isotope anomalies most likely reflect the heterogeneous distribution of the same *s*-process carrier. Presolar SiC grains are strongly enriched in *s*-process nuclides (Hoppe and Ott, 1997) and would therefore be an obvious candidate for the carrier phase that causes the isotopic variability among the chondrules and between chondrules and matrix. However, unlike Mo and W, there are no resolvable Ba isotope anomalies between chondrules and matrix (Fig. 3b), although such anomalies would be expected for the heterogeneous distribution of SiC. This is because SiC grains exhibit strong depletions in ^{135}Ba (e.g., Prombo et al., 1993), and so the chondrules should have ^{135}Ba excesses if their *s*-process deficit would reflect the depletion of presolar SiC. To assess the magnitude of this effect, we calculated the expected ^{135}Ba and ^{183}W variations resulting from the heterogeneous distribution of presolar SiC. One problem with these calculations is that trace element concentrations in SiC are often not well known. For instance, reported Ba concentrations in SiC vary from ~2 to ~200 ppm (Ávila et al., 2013; Zinner et al., 1991). We therefore used Ba and W concentrations reported for the same set of presolar SiC grains and determined using the same analytical method (Ávila et al., 2012, 2013). However, for this set of samples, no Mo concentration data are available, and so we could not calculate the collateral effects on Mo isotopes. The calculations show that producing the largest ^{183}W anomaly of the chondrule separates ($\varepsilon^{183}\text{W} \approx 2.3$ for sample C3i) by a deficit in presolar SiC grains would lead to a collateral Ba isotopic anomaly of $\varepsilon^{135}\text{Ba} \approx 1.0$ (Fig. 3b). However, this chondrule sample has $\varepsilon^{135}\text{Ba} = 0.21 \pm 0.13$ (Table 1), essentially the same value as all other samples of this study. These calculations thus show that if the W isotope anomalies were caused by variable proportions of presolar SiC, then the chondrule and matrix samples should exhibit resolved ε^{135}Ba anomalies. However, all these samples have indistinguishable Ba isotopic compositions, which are also indistinguishable from that of bulk Allende (Table S4). Thus, the observed Mo and W isotope anomalies are difficult to reconcile with an uneven distribution of presolar SiC (Fig. 3b).

The three separates of chondrule fraction C3 show a large spread in Mo isotope anomalies with ε^{92}Mo values between ~3.6 and ~7.5 (Table 1), and exhibit an inverse correlation between ε^{92}Mo and magnetic susceptibility, where the non-magnetic fraction (C3n) has the largest and the magnetic fraction (C3m) has the smallest anomaly (Fig. 4). The non-magnetic fraction C3n, therefore, has a larger *s*-deficit than the magnetic fraction C3m; consequently, the magnetic chondrule fraction is enriched in an *s*-process carrier compared to the non-magnetic fraction C3n (note that all chondrules are depleted in this carrier relative to the matrix). Hence, the abundance of the presolar carrier is positively correlated with the abundance of magnetic components, which in case of Allende chondrules are Fe–Ni metal, magnetite, and pyrrhotite (Emmerton et al., 2011). Of these, magnetite is the most abundant magnetic phase and thus the dominant factor controlling the magnetic susceptibility of the chondrules. Magnetite in Allende chondrules predominantly formed by oxidation of Fe–Ni metal during parent body processes (Choi et al., 1997; Krot et al., 1995); thus, the abundance of the *s*-carrier is correlated with the initial (i.e., at the time of chondrule formation) metal content of the chondrules, where 'metal-rich' chondrules are enriched in an *s*-process carrier compared to 'metal-poor' chondrules. The *s*-process Mo therefore most likely is hosted in a presolar metal carrier, although we cannot exclude other carriers that are likely to be associated with metal, such as some sulfides and oxides. Of note, such grains do not contain significant amounts of Ba, consistent with the absence of Ba isotopic anomalies in the analyzed chondrule and matrix samples.

All chondrule and matrix fractions plot on single ε^{i}Mo–ε^{92}Mo correlation lines (Fig. 2), strongly suggesting that both the *s*-process variability between chondrules and matrix as well as the vari-

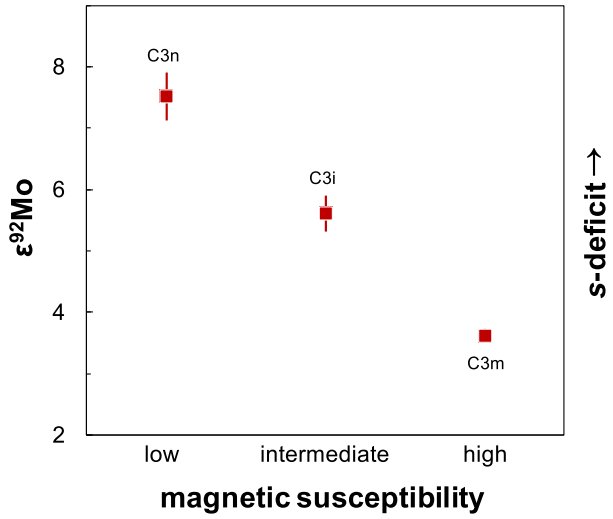

Fig. 4. ε^{92}Mo values for the three separates of chondrule fraction C3 as a function of their magnetic susceptibility. Non-magnetic fraction C3n has the highest, while magnetic fraction C3m has the lowest ε^{92}Mo anomaly. The inverse correlation of the deficit in *s*-process Mo with magnetic susceptibility indicates that the *s*-deficit is caused by the depletion of an *s*-carrier that is associated with magnetic components (metal, sulfides, oxides). See Section 4.2 for details.

able *s*-deficits in the different chondrule fractions are caused by the heterogeneous distribution of the same *s*-process carrier. The *s*-excess observed for the matrix would thus result from the enrichment of an *s*-carrier that is associated with metal. This interpretation is consistent with the general observation that matrix is enriched in metal over chondrules, as is evident from the enrichment of siderophile elements in the matrix (e.g., Palme et al., 2014b). Collectively, these observations suggest that the isotopic complementarity of chondrules and matrix results from metal–silicate separation during chondrule formation.

4.3. Origin of chondrules

The depletion of *s*-process Mo (and W) in chondrules and the complementary enrichment of this material in the matrix have important implications for understanding the origin of chondrules. However, before the isotopic data can be used to assess chondrule formation models, it is important to consider the potential effects of incomplete dissolution and parent body processes (i.e., aqueous alteration, thermal metamorphism) on the isotopic compositions measured for chondrules and matrix. Presolar grains (e.g., SiC) can be extremely acid-resistant and so incomplete acid dissolution of such grains can lead to measured isotopic compositions that reflect a deficit in the incompletely dissolved presolar component (Brandon et al., 2005; Yokoyama et al., 2007). However, several lines of evidence indicate that the nucleosynthetic Mo isotope variations observed for chondrules and matrix do not reflect the incomplete dissolution of acid-resistant presolar grains. First, chondrules do not contain presolar grains, and so their deficit in *s*-process Mo cannot result from incomplete sample digestion but must be an inherent feature of the chondrules. Second, incomplete dissolution cannot account for the complementary isotope anomalies in chondrules and matrix, which reflect the enrichment and complementary depletion of a single presolar carrier. Finally, the matrix is characterized by an excess of *s*-process Mo, but incomplete digestion can only result in an apparent deficit, and not an excess, in the nucleosynthetic component present in the presolar grains that would not have been completely dissolved.

The Mo isotope anomalies are also unlikely to be the result of parent body processes such as aqueous alteration or thermal metamorphism. These processes tend to decrease and not increase the magnitude of nucleosynthetic isotope anomalies because they potentially result in the redistribution and homogenization of isotopically heterogeneous materials (Yokoyama et al., 2011). Moreover, the Mo isotopic data indicate the enrichment of an *s*-process carrier in the matrix and the complementary depletion of that carrier in the chondrules. To explain this complementarity by parent body processes, one would need to argue for the release of *s*-process material from the chondrules and the preferential incorporation of this material into the matrix. However, chondrules do not contain presolar grains and so it is not possible to redistribute isotopically anomalous material released from chondrules into the matrix. In summary, neither the incomplete dissolution of presolar grains nor parent body processes can account for the complementary enrichment and depletion of *s*-process material in matrix and chondrules, indicating that these isotopic signatures are genuine features established during chondrule formation. Thus, the isotopic data can be used to assess the origin of chondrules.

Recently, a series of models has been developed in which chondrules formed during protoplanetary impacts (e.g., Asphaug et al., 2011; Johnson et al., 2015; Sanders and Scott, 2012). In its original form, the impact model posits that chondrules originated as splashes expelled by the collision of molten planetesimals (Sanders, 1996; Sanders and Scott, 2012; Zook, 1981). However, several lines of evidence indicate that this model cannot account for the isotopic compositions of chondrules and matrix. First, chondrules exhibit larger nucleosynthetic Mo and W isotope anomalies than observed for bulk, differentiated meteorites. Second, different chondrule populations from Allende show variable nucleosynthetic Mo isotope anomalies, indicating that they do not derive from a homogeneous reservoir of melt. Thus, an origin of chondrules as melt splashes from differentiated planetesimals is inconsistent with the observed nucleosynthetic isotope anomalies for chondrules. Finally, this impact model also does not provide a mechanism to enrich an *s*-process carrier in the matrix and deplete the same carrier in the chondrules.

More recent versions of the impact model for the origin of chondrules invoke collisions of planetesimals that are either undifferentiated or maintained a primitive, un-melted crust (Johnson et al., 2015). However, these models are also inconsistent with the isotopic data, because it is highly unlikely that impact melting produced melt droplets that are variably depleted in a presolar *s*-carrier. Moreover, these melt droplets would have to be re-mixed with un-melted dust (i.e., the matrix) that contained the complementary proportion of this *s*-carrier to yield the observed isotopic composition of the bulk meteorite. This is particularly problematic for the observed W isotope systematics, because nucleosynthetic W isotope anomalies in bulk meteorites are minor to absent, yet chondrules and matrix show large and complementary nucleosynthetic W isotope anomalies (Budde et al., 2016). Thus, chondrules and matrix must always be mixed in the exactly right proportions to maintain the bulk inner solar system W isotopic composition (Budde et al., 2016).

In contrast to the impact models, the formation of chondrules and matrix from the same reservoir of solar nebula dust is consistent with the isotopic constraints. The Mo isotope data show that during the melting of dust that produced chondrules, a carrier of *s*-process Mo (and W) must have been preferentially incorporated into the matrix over chondrules. This uneven distribution of a presolar component could in principle reflect either the sorting of presolar grains according to their size or type, or the preferential exclusion of such grains during the melting that produced the chondrules (Budde et al., 2016). As argued above, the *s*-process carrier responsible for the nucleosynthetic isotope anomalies in chondrules and matrix probably is associated with metal. Thus, one possibility is that there had been metal–silicate separation just

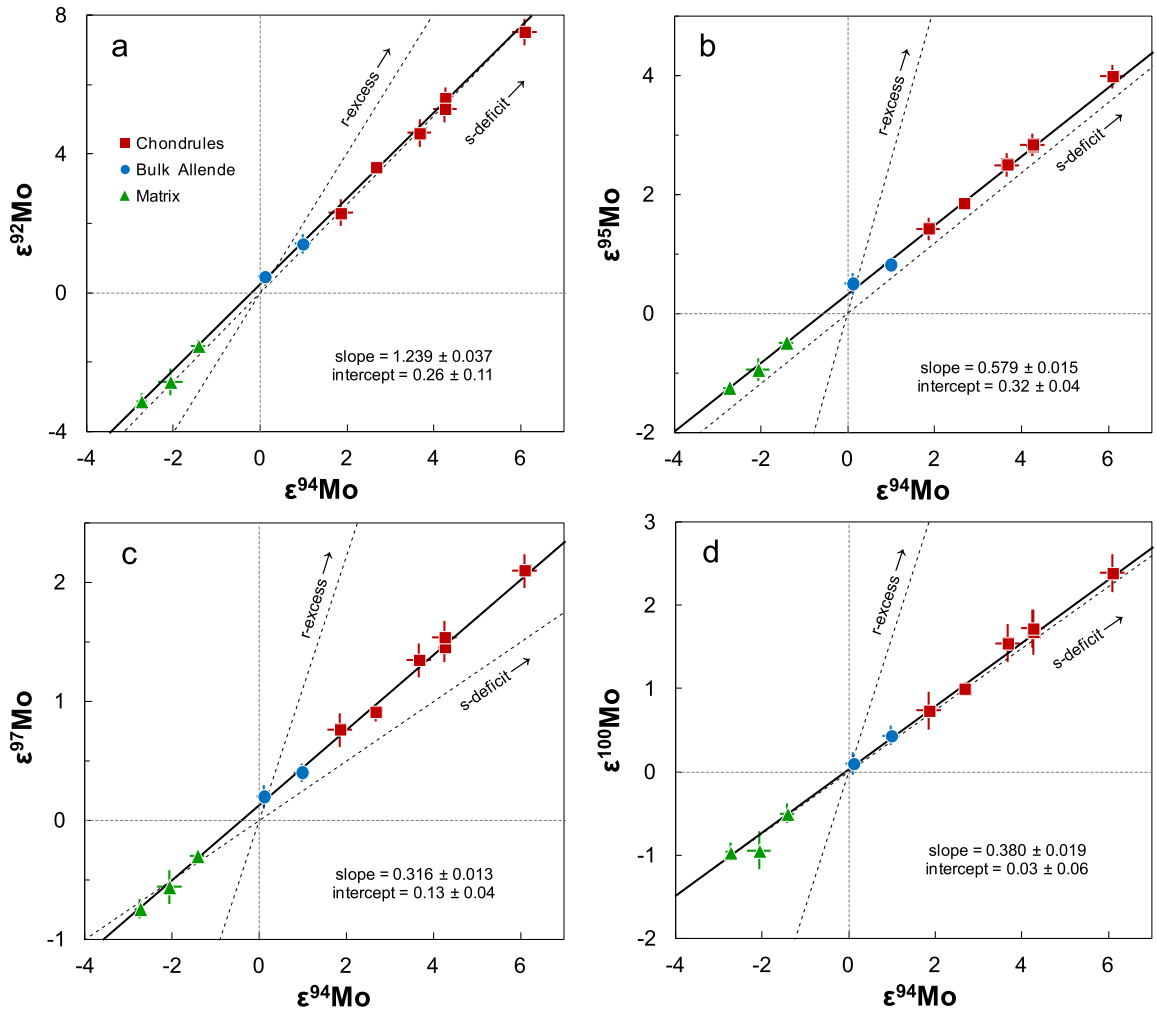

Fig. 5. Plots of ε^{i}Mo versus ε^{94}Mo for the Allende samples. Dashed lines are mixing lines between terrestrial and *s*- and *r*-process Mo (see Fig. 2); solid lines indicate regressions through the chondrule and matrix samples (see Fig. 2). The correlation lines reveal resolved positive intercepts for ε^{92}Mo, ε^{95}Mo, and ε^{97}Mo, but not for ε^{100}Mo. This offset is most clearly seen in the ε^{95}Mo–ε^{94}Mo plot (b), in which the Allende chondrule and matrix samples plot on a line that is parallel to the mixing line between terrestrial and *s*-process Mo.

prior to the formation of chondrules from 'metal-poor' dust aggregates. For instance, Hubbard (2016) argued that ferromagnetic interactions between dust grains facilitated metal–silicate separation and led to the preferential melting of metal-poor dust aggregates which became chondrules. Another possibility is that the carrier of *s*-process Mo and W was preferentially excluded from the melting that produced the chondrules. The liquidus temperatures of chondrules were in the range 1350–1800 °C (Cohen et al., 2000) and, therefore, were at least partly lower than the melting temperature of pure Fe metal. Thus, it is conceivable that some of the metal grains did not melt during chondrule formation and were, therefore, excluded from the chondrules and incorporated into the matrix.

In summary, the complementary nucleosynthetic isotope anomalies in chondrules and matrix, together with the chemical complementarity observed in prior studies, refute an origin of chondrules by protoplanetary impacts and instead require a solar nebula origin of chondrules. The isotopic data indicate that the enrichment of an *s*-process carrier in the matrix over chondrules was associated with metal–silicate fractionation during chondrule formation, and require that chondrules and matrix formed together from a common reservoir of solar nebula dust.

5. Mo isotope dichotomy between carbonaceous and non-carbonaceous meteorites

5.1. Two distinct Mo isotope reservoirs in the solar nebula

The Allende chondrule and matrix data fall on single, well-defined ε^{i}Mo–ε^{92}Mo correlation lines, which pass through the terrestrial composition for ε^{100}Mo, but not for ε^{94}Mo, ε^{95}Mo, and ε^{97}Mo (Fig. 2). These non-terrestrial intercepts are more clearly seen when the ε^{i}Mo data are plotted against ε^{94}Mo. In these plots, resolved excesses are observed for ε^{92}Mo, ε^{95}Mo, and ε^{97}Mo, but not for ε^{100}Mo (Fig. 5). The offset of the correlation line defined by Allende chondrules and matrix from the *s*-mixing line passing through the terrestrial Mo isotope composition is largest in the ε^{95}Mo–ε^{94}Mo plot, in which the difference between *s*- and *r*-process slopes is most pronounced (Fig. 5b). Of note, acid leachates of the Murchison and Orgueil chondrites (Burkhardt et al., 2012; Dauphas et al., 2002b) plot on the chondrule–matrix ε^{95}Mo–ε^{94}Mo correlation line (Fig. S4), and the linear regression of the leachate data also gives a positive ε^{95}Mo-intercept of 0.32 ± 0.11 at $\varepsilon^{94}\text{Mo} = 0$. Thus, the non-terrestrial intercepts observed for Allende chondrules and matrix seem to be a characteristic feature of carbonaceous chondrites in general, consistent with the observation that bulk carbonaceous chondrites also plot on the

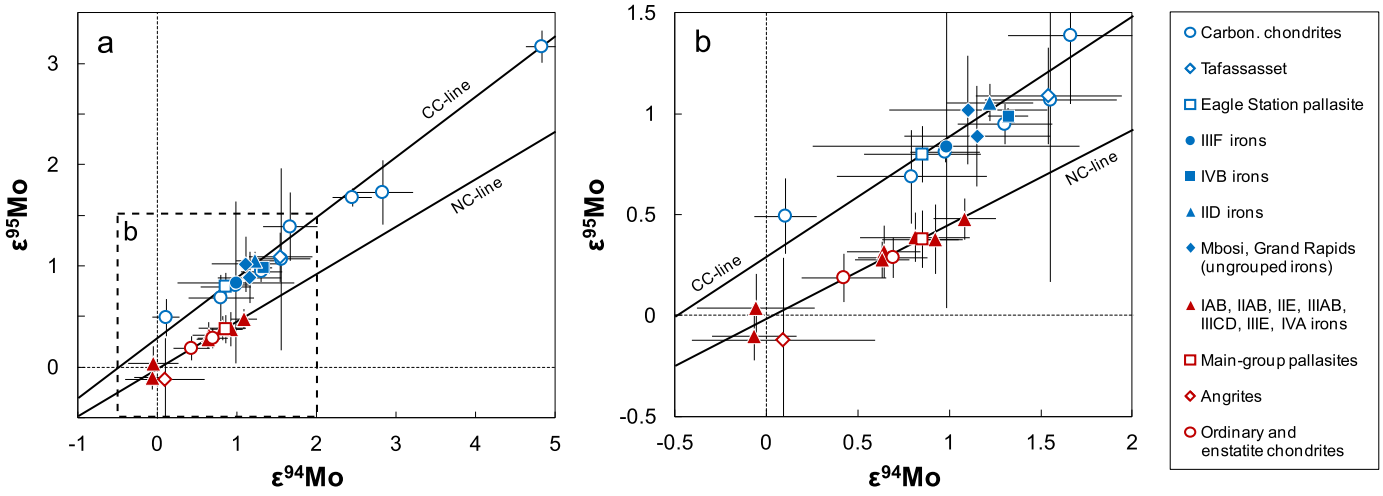

Fig. 6. Plot of ε^{95}Mo versus ε^{94}Mo for bulk meteorites. Carbonaceous (blue, CC-line) and non-carbonaceous (red, NC-line) meteorites plot on separate *s*-mixing lines. For the division of meteorites in carbonaceous and non-carbonaceous meteorites see Table 2. Most bulk meteorite data are from Burkhardt et al. (2011), except for CK and CO (Burkhardt et al., 2014), IID (Fischer-Gödde et al., 2016), and Grand Rapids (Dauphas et al., 2002a). (For interpretation of the references to color in this figure legend, the reader is referred to the web version of this article.)

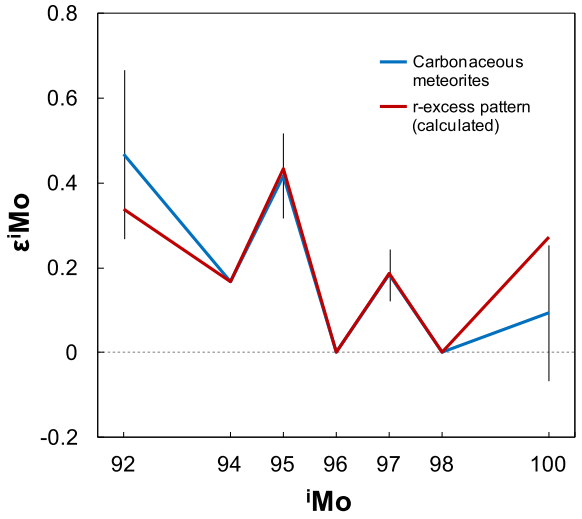

Fig. 7. Comparison of the Mo isotope excess of carbonaceous meteorites as determined from the intercepts of ε^{i}Mo–ε^{94}Mo correlation lines defined by Allende chondrules and matrix (blue) to the Mo isotopic pattern expected for the addition of pure *r*-excess matter (red). The *r*-process composition was obtained from the *r*-residuals, calculated by subtracting the *s*-process abundances obtained from Mo isotope data for SiC grains (Nicolussi et al., 1998) from the terrestrial Mo isotope abundances (note that ^{92}Mo and ^{94}Mo are not produced in the *r*-process). (For interpretation of the references to color in this figure legend, the reader is referred to the web version of this article.)

ε^{95}Mo–ε^{94}Mo correlation line defined by the chondrule and matrix data (Fig. 6 and Section 5.2).

The *r*- and *s*-mixing lines plotted in Fig. 5 show that the offset of the *s*-mixing line defined by carbonaceous chondrites can be attributed to the addition of a component enriched in *r*-process Mo isotopes. To test this idea, we calculated the Mo isotope effects expected for the addition of pure *r*-process matter and compared them to the observed Mo isotope excesses obtained from the intercepts of the chondrule–matrix regressions (Fig. 7). The results of these calculations show that the predicted and observed Mo isotope patterns are in good agreement and that only for ε^{100}Mo a larger excess would be expected (Fig. 7). Nevertheless, within uncertainty both the calculated and observed ε^{100}Mo values overlap. Thus, the offset of the *s*-mixing line of the carbonaceous chondrites from an *s*-mixing line passing through the terrestrial Mo isotope composition is consistent with the addition of *r*-process matter to the carbonaceous chondrites.

The carrier of this *r*-process material is difficult to determine. One possibility is that this material was carried by CAIs, many of which are characterized by an excess in *r*-process Mo isotopes (Brennecka et al., 2013; Burkhardt et al., 2011). However, different groups of carbonaceous chondrites have very different CAI abundances, yet they all exhibit a uniform *r*-excess. Thus, the *r*-excess of the carbonaceous meteorites does not seem to be related to the presence of CAIs, but more likely reflects the addition of presolar grains enriched in *r*-process nuclides. Another possibility is that this added material was not pure *r*-process matter, but was material from a supernova neutron burst. Theoretical calculations reveal that a neutron burst produces excesses in ^{95}Mo and ^{97}Mo without producing similar excesses in ^{100}Mo (Meyer et al., 2000). Such compositions have been measured for presolar type X SiC grains, which are thought to have condensed in the interior of expanding supernovae (e.g., Nittler et al., 1996). These X grains are characterized by ^{95}Mo and ^{97}Mo excesses but show no ^{100}Mo excess (Pellin et al., 2000), consistent with the observation that for the carbonaceous chondrites we observe no resolvable excess for ε^{100}Mo. Nevertheless, distinguishing between pure *r*-process and neutron burst material will require more precise ε^{100}Mo data for the carbonaceous meteorites. However, regardless of the exact nature of the added presolar component, this material evidently was produced in a supernova environment.

An important observation from Fig. 6 is that bulk carbonaceous chondrites (CCs) plot on the correlation line defined by chondrules and matrix as well as the acid leachate data. In contrast, ordinary (OCs) and enstatite (ECs) chondrites as well as most iron meteorites do not fall on this line, but plot on a separate *s*-mixing line that passes through the origin (i.e., through the terrestrial composition at ε^{94}Mo and ε^{95}Mo = 0) (Fig. 6). A linear regression of all carbonaceous chondrite data (i.e., Allende chondrule and matrix fractions, acid leachates, and bulk samples) yields ε^{95}Mo = $(0.596 \pm 0.006) \times \varepsilon^{94}$Mo + (0.29 ± 0.03); we term this line the 'CC-line' (Carbonaceous Chondrite-line). A linear regression of the other, non-carbonaceous meteorites (i.e., enstatite and ordinary chondrites; IAB, IIAB, IIE, IIIAB, IIICD, IIIE, and IVA irons) yields ε^{95}Mo = $(0.47 \pm 0.14) \times \varepsilon^{94}$Mo − (0.02 ± 0.10); we term this line the 'NC-line' (Non-Carbonaceous-line). The slopes of the NC- and CC-lines appear to be slightly different, although this difference is not resolved. Of note, the slope of the CC-line is in

Table 2
Classification of meteorites based on Mo isotopes.

		Carbonaceous meteorites	Non-carbonaceous meteorites
Undifferentiated meteorites	Chondrites	CI, CM, CV, CR, CB, CO, CK	OC (H, L, LL), EC (EH, EL)
Differentiated meteorites	Iron meteorites	IID, IIIF, IVB, Mbosi, Grand Rapids	IAB, IIAB, IIE, IIIAB, IIICD, IIIE, IVA
	Stony iron meteorites	Eagle Station pallasite	Main-group pallasites
	Achondrites	Tafassasset	Angrites
ε^{95}Mo–ε^{94}Mo correlation		$\varepsilon^{95}\text{Mo} = (0.596 \pm 0.006) \times \varepsilon^{94}\text{Mo} + (0.29 \pm 0.03)$	$\varepsilon^{95}\text{Mo} = (0.47 \pm 0.14) \times \varepsilon^{94}\text{Mo} - (0.02 \pm 0.10)$

Classification is based on Mo isotope data for bulk meteorites from Burkhardt et al. (2011); except for CK and CO (Burkhardt et al., 2014), IID (Fischer-Gödde et al., 2016), and Grand Rapids (Dauphas et al., 2002a). See Section 5.1 and Fig. 6 for further details.

very good agreement with that calculated based on the *s*-process Mo composition measured in SiC grains (Nicolussi et al., 1998), which gives $\varepsilon^{95}\text{Mo}/\varepsilon^{94}\text{Mo} = 0.59 \pm 0.02$ (Dauphas et al., 2004). The slope of the NC-line also overlaps with this value, indicating that the Mo isotope variations within both the carbonaceous and non-carbonaceous meteorite groups are caused by the uneven distribution of *s*-process material (Fig. 6). As to whether these variations can be attributed to the same or different carriers of *s*-process Mo is unclear at present, because the slopes of the CC- and NC-lines are not clearly resolved from each other.

5.2. Carbonaceous and non-carbonaceous meteorites

The presence of two distinct *s*-mixing lines in a plot of ε^{95}Mo versus ε^{94}Mo (Fig. 6) offers a new means to assess the genetic heritage of meteorites and to distinguish whether a given meteorite parent body assembled from carbonaceous or non-carbonaceous material. This distinction was previously proposed by Warren (2011), who also observed this dichotomy based on nucleosynthetic Cr and Ti isotope anomalies. Of note, carbonaceous meteorites exhibit ubiquitous ^{54}Cr excesses (Shukolyukov and Lugmair, 2006; Trinquier et al., 2007), the carrier of which probably are small nanospinels formed in supernovae (Dauphas et al., 2010; Qin et al., 2011). Thus, both the Cr and Mo isotopic data indicate an excess of supernova material in the carbonaceous over the non-carbonaceous meteorites. The advantage of Mo is that it can, unlike Cr and Ti, readily be analyzed in iron meteorites, making it possible to establish links between specific iron meteorite groups and carbonaceous or non-carbonaceous meteorites. As illustrated in Fig. 6, most iron meteorites belong to the non-carbonaceous meteorites, whereas the IVB, IID, IIIF, and some ungrouped irons as well as the Eagle Station pallasite and Tafassasset plot on the CC-line and, therefore, are genetically linked to carbonaceous chondrites (Table 2). Note that a link of the IVB irons and the Eagle Station pallasite to carbonaceous chondrites has previously been proposed based on Ni (Regelous et al., 2008) and Cr isotopic data (Shukolyukov and Lugmair, 2006).

An important observation from the Mo isotopic data is that the carbonaceous and non-carbonaceous meteorite groups both contain iron meteorites. Those belonging to the carbonaceous meteorites (groups IID and IVB) have younger Hf–W model ages of core formation (~2.9 Ma after CAI formation) than irons belonging to the non-carbonaceous groups (IIAB, IIIAB, and IVA), whose Hf–W model ages are between ~0.7 and ~1.4 Ma after CAI formation (Kruijer et al., 2014). This difference in core formation ages might reflect the low S contents and, hence, high melting temperatures of the IID and IVB irons (Kruijer et al., 2014). However, in light of our finding of a distinct heritage of these two groups of iron meteorites, the difference in core formation ages may also reflect a slightly later accretion of the IID and IVB parent bodies compared to the parent bodies of the non-carbonaceous iron meteorites. Kruijer et al. (2014) showed that based on the difference in core formation ages, the IID and IVB parent bodies might have accreted ~0.5 Ma later than those of the IIAB, IIIAB, and IVA irons. Such later accretion would be consistent with the idea that carbonaceous meteorites formed at greater heliocentric distance than non-carbonaceous meteorites (e.g., Warren, 2011; Wood, 2005), where accretion might have been slower.

5.3. Implications for the early solar nebula and formation of the gas giants

A striking observation from the Mo isotope data is that the meteorites form two distinct clusters of compositions, as manifested by the presence of two nearly parallel correlation lines in the ε^{95}Mo–ε^{94}Mo plot (i.e., the CC- and NC-lines). There does not seem to be meteoritic material plotting between these two lines, suggesting limited mixing between the carbonaceous and non-carbonaceous reservoirs. Moreover, because the carbonaceous meteorites and their components (excluding CAIs) plot on a single *s*-mixing line, they all have approximately the same ^{95}Mo (and ^{97}Mo) excess relative to the NC-line (Fig. 6). Thus, the supernova material carrying these excesses must have been added to and homogeneously distributed within the carbonaceous meteorite reservoir before formation of the first bodies within this reservoir. Based on Hf–W chronometry, Kruijer et al. (2014) have shown that the IID and IVB parent bodies probably accreted within <1 Ma after CAI formation, indicating that the added supernova material had been homogenized within the carbonaceous meteorite region by this time at the latest. Likewise, accretion of bodies in the non-carbonaceous meteorite region also started early, probably within ~0.3 Ma after CAI formation (Kruijer et al., 2014). In both regions, meteorite parent body accretion continued for at least ~2 Ma, as is evident from ages for chondrules from ordinary and carbonaceous chondrites (e.g., Budde et al., 2016; Connelly et al., 2012; Kita et al., 2013). Thus, the distinct compositions of carbonaceous and non-carbonaceous meteorites were established early and both reservoirs coexisted in spatially distinct areas in the solar nebula for at least ~2 Ma.

The limited mixing between the non-carbonaceous and carbonaceous meteorites indicates that these two solar nebula reservoirs were separated by a large distance, implying that material located in between these two reservoirs was not sampled by meteorites and, hence, probably is not present in the asteroid belt. Thus, the Mo isotopic data indicate that the asteroid belt as sampled by meteorites consists of two distinct populations of bodies, derived from two separate nebular source regions (the NC- and CC-reservoirs), which initially were far apart from each other. This observation is consistent with several aspects of the *Grand Tack* model of early solar system evolution. This model invokes an inward-then-outward migration of Jupiter and Saturn, leading to an early depletion of bodies located between approximately 4 and 6 AU (Walsh et al., 2011). In this model, the asteroid belt was subsequently repopulated with bodies from two distinct sources, one from inside Jupiter and the other from beyond Jupiter. Thus, the Grand Tack model not only is consistent with the observed Mo

isotope dichotomy between non-carbonaceous and carbonaceous meteorites, but it also provides a mechanism for keeping these two reservoirs separate from each other.

6. Conclusions

Chondrules from the Allende chondrite are variably depleted in a presolar component (most likely metal grains) that is enriched in *s*-process Mo and W nuclides. The same carrier is enriched in the matrix, leading to complementary nucleosynthetic isotope anomalies in chondrules and matrix. This uneven distribution of presolar matter was most likely produced during metal–silicate fractionation accompanying chondrule formation and may be related to magnetic interactions of dust grains or the exclusion of metal grains enriched in *s*-process matter from the melting that produced the chondrules. Regardless of its exact origin, the isotopic complementarity requires that chondrules and matrix formed together from the same reservoir of solar nebula dust, and indicates that chondrules did not form by protoplanetary impacts. The isotopic data do not rule out that some specific types of chondrules, such as those in CB chondrites, originated in impacts (Krot et al., 2005), but the majority of chondrules must have had a solar nebula origin.

Allende chondrules and matrix as well as bulk carbonaceous chondrites show a uniform excess in ^{95}Mo (as well as ^{92}Mo and ^{97}Mo), resulting from the addition of supernova material (either pure *r*-process or neutron burst material). Enstatite and ordinary chondrites and most iron meteorites do not contain this material, demonstrating that two distinct Mo isotope reservoirs co-existed in the early solar nebula that remained spatially separated for several million years. This separation was most likely achieved through the formation of Jupiter, which cleared the disk between the inner and outer solar system regions parental to the non-carbonaceous and carbonaceous meteorites. Subsequent mixing between these two reservoirs probably occurred through the outward migration of Jupiter, which resulted in scattering of bodies that had originally formed beyond the orbit of Jupiter into the inner solar system. Thus, the Mo isotopic data provide evidence for the existence of the two distinct source regions of asteroids predicted in the Grand Tack model.

The Mo isotope dichotomy of meteorites provides a new means to assess genetic links between chondrites and differentiated meteorites, as has previously been done using mainly anomalies in O isotopes and ^{54}Cr. The Mo isotope anomalies are particularly useful, because unlike Cr they can readily be analyzed in iron meteorites. Thus, when Cr and Mo isotopes are used in concert, the genetic heritage of essentially every meteorite can be determined, making such data a valuable addition to current meteorite classification schemes.

Acknowledgements

We thank K. Mezger and D.C. Hezel for constructive reviews and B. Marty for his editorial efforts. We are grateful to J. Render for assistance with lab work and MC-ICP-MS measurements, U. Heitmann for assistance with sample preparation, and D. Ebel, A. Hubbard, and K. Metzler for discussions. This study was supported by the Deutsche Forschungsgemeinschaft (DFG) as part of the SPP 1385 “The First 10 Million Years of the Solar System – a Planetary Materials Approach” (grants KL 1857/3 and KL 1857/4 to T.K.). C.B. was supported by the European Research Council Consolidator Grant ‘ISOCORE’ (616564 to T.K.). Acquisition of the TIMS was made possible through support from a Sofja Kovalevskaja award from the Alexander von Humboldt Foundation (G.A.B.). These sources of funding are gratefully acknowledged.

Appendix A. Supplementary material

Supplementary material related to this article can be found online at http://dx.doi.org/10.1016/j.epsl.2016.09.020.

References

Arlandini, C., Käppeler, F., Wisshak, K., Gallino, R., Lugaro, M., Busso, M., Straniero, O., 1999. Neutron capture in low-mass asymptotic giant branch stars: cross sections and abundance signatures. Astrophys. J. 525, 886–900. http://dx.doi.org/10.1086/307938.

Asphaug, E., Jutzi, M., Movshovitz, N., 2011. Chondrule formation during planetesimal accretion. Earth Planet. Sci. Lett. 308, 369–379. http://dx.doi.org/10.1016/j.epsl.2011.06.007.

Ávila, J.N., Ireland, T.R., Gyngard, F., Zinner, E., Mallmann, G., Lugaro, M., Holden, P., Amari, S., 2013. Ba isotopic compositions in stardust SiC grains from the Murchison meteorite: insights into the stellar origins of large SiC grains. Geochim. Cosmochim. Acta 120, 628–647. http://dx.doi.org/10.1016/j.gca.2013.03.039.

Ávila, J.N., Lugaro, M., Ireland, T.R., Gyngard, F., Zinner, E., Cristallo, S., Holden, P., Buntain, J., Amari, S., Karakas, A., 2012. Tungsten isotopic compositions in stardust SiC grains from the Murchison meteorite: constraints on the s-process in the Hf-Ta-W-Re-Os region. Astrophys. J. 744, 49. http://dx.doi.org/10.1088/0004-637X/744/1/49.

Becker, M., Hezel, D.C., Schulz, T., Elfers, B.-M., Münker, C., 2015. Formation timescales of CV chondrites from component specific Hf–W systematics. Earth Planet. Sci. Lett. 432, 472–482. http://dx.doi.org/10.1016/j.epsl.2015.09.049.

Bermingham, K.R., Mezger, K., Scherer, E.E., Horan, M.F., Carlson, R.W., Upadhyay, D., Magna, T., Pack, A., 2016. Barium isotope abundances in meteorites and their implications for early Solar System evolution. Geochim. Cosmochim. Acta 175, 282–298. http://dx.doi.org/10.1016/j.gca.2015.11.006.

Bland, P.A., Alard, O., Benedix, G.K., Kearsley, A.T., Menzies, O.N., Watt, L.E., Rogers, N.W., 2005. Volatile fractionation in the early solar system and chondrule/matrix complementarity. Proc. Natl. Acad. Sci. USA 102, 13755–13760. http://dx.doi.org/10.1073/pnas.0501885102.

Brandon, A.D., Humayun, M., Puchtel, I.S., Leya, I., Zolensky, M., 2005. Osmium isotope evidence for an *s*-process carrier in primitive chondrites. Science 309, 1233–1236. http://dx.doi.org/10.1126/science.1115053.

Brennecka, G.A., Borg, L.E., Wadhwa, M., 2013. Evidence for supernova injection into the solar nebula and the decoupling of *r*-process nucleosynthesis. Proc. Natl. Acad. Sci. USA 110, 17241–17246. http://dx.doi.org/10.1073/pnas.1307759110.

Budde, G., Kleine, T., Kruijer, T.S., Burkhardt, C., Metzler, K., 2016. Tungsten isotopic constraints on the age and origin of chondrules. Proc. Natl. Acad. Sci. USA 113, 2886–2891. http://dx.doi.org/10.1073/pnas.1524980113.

Burkhardt, C., Hin, R.C., Kleine, T., Bourdon, B., 2014. Evidence for Mo isotope fractionation in the solar nebula and during planetary differentiation. Earth Planet. Sci. Lett. 391, 201–211. http://dx.doi.org/10.1016/j.epsl.2014.01.037.

Burkhardt, C., Kleine, T., Dauphas, N., Wieler, R., 2012. Origin of isotopic heterogeneity in the solar nebula by thermal processing and mixing of nebular dust. Earth Planet. Sci. Lett. 357–358, 298–307. http://dx.doi.org/10.1016/j.epsl.2012.09.048.

Burkhardt, C., Kleine, T., Oberli, F., Pack, A., Bourdon, B., Wieler, R., 2011. Molybdenum isotope anomalies in meteorites: constraints on solar nebula evolution and origin of the Earth. Earth Planet. Sci. Lett. 312, 390–400. http://dx.doi.org/10.1016/j.epsl.2011.10.010.

Carlson, R.W., Boyet, M., Horan, M., 2007. Chondrite barium, neodymium, and samarium isotopic heterogeneity and early Earth differentiation. Science 316, 1175–1178. http://dx.doi.org/10.1126/science.1140189.

Choi, B.-G., McKeegan, K.D., Leshin, L.A., Wasson, J.T., 1997. Origin of magnetite in oxidized CV chondrites: in situ measurement of oxygen isotope compositions of Allende magnetite and olivine. Earth Planet. Sci. Lett. 146, 337–349. http://dx.doi.org/10.1016/S0012-821X(96)00229-4.

Cohen, B.A., Hewins, R.H., Yu, Y., 2000. Evaporation in the young solar nebula as the origin of ‘just-right’ melting of chondrules. Nature 406, 600–602. http://dx.doi.org/10.1038/35020514.

Connelly, J.N., Bizzarro, M., Krot, A.N., Nordlund, Å., Wielandt, D., Ivanova, M.A., 2012. The absolute chronology and thermal processing of solids in the solar protoplanetary disk. Science 338, 651–655. http://dx.doi.org/10.1126/science.1226919.

Dauphas, N., Davis, A.M., Marty, B., Reisberg, L., 2004. The cosmic molybdenum–ruthenium isotope correlation. Earth Planet. Sci. Lett. 226, 465–475. http://dx.doi.org/10.1016/j.epsl.2004.07.026.

Dauphas, N., Marty, B., Reisberg, L., 2002a. Molybdenum evidence for inherited planetary scale isotope heterogeneity of the protosolar nebula. Astrophys. J. 565, 640–644. http://dx.doi.org/10.1086/324597.

Dauphas, N., Marty, B., Reisberg, L., 2002b. Molybdenum nucleosynthetic dichotomy revealed in primitive meteorites. Astrophys. J. 569, L139–L142. http://dx.doi.org/10.1086/340580.

Dauphas, N., Remusat, L., Chen, J.H., Roskosz, M., Papanastassiou, D.A., Stodolna, J., Guan, Y., Ma, C., Eiler, J.M., 2010. Neutron-rich chromium isotope anomalies in supernova nanoparticles. Astrophys. J. 720, 1577–1591. http://dx.doi.org/10.1088/0004-637X/720/2/1577.

Dauphas, N., Schauble, E.A., 2016. Mass fractionation laws, mass-independent effects, and isotopic anomalies. Annu. Rev. Earth Planet. Sci. 44, 709–783. http://dx.doi.org/10.1146/annurev-earth-060115-012157.

Ebel, D.S., Brunner, C., Konrad, K., Leftwich, K., Erb, I., Lu, M., Rodriguez, H., Crapster-Pregont, E.J., Friedrich, J.M., Weisberg, M.K., 2016. Abundance, major element composition and size of components and matrix in CV, CO and Acfer 094 chondrites. Geochim. Cosmochim. Acta 172, 322–356. http://dx.doi.org/10.1016/j.gca.2015.10.007.

Emmerton, S., Muxworthy, A.R., Hezel, D.C., Bland, P.A., 2011. Magnetic characteristics of CV chondrules with paleointensity implications. J. Geophys. Res. 116, E12007. http://dx.doi.org/10.1029/2011JE003856.

Fischer-Gödde, M., Render, J., Budde, G., Burkhardt, C., Kleine, T., 2016. Molybdenum isotope dichotomy of meteorites. Goldschmidt Conference. #4380.

Hezel, D.C., Palme, H., 2008. Constraints for chondrule formation from Ca–Al distribution in carbonaceous chondrites. Earth Planet. Sci. Lett. 265, 716–725. http://dx.doi.org/10.1016/j.epsl.2007.11.003.

Hezel, D.C., Palme, H., 2010. The chemical relationship between chondrules and matrix and the chondrule matrix complementarity. Earth Planet. Sci. Lett. 294, 85–93. http://dx.doi.org/10.1016/j.epsl.2010.03.008.

Hoppe, P., Ott, U., 1997. Mainstream silicon carbide grains from meteorites. AIP Conf. Proc. 402, 27–58. http://dx.doi.org/10.1063/1.53314.

Hubbard, A., 2016. Partitioning tungsten between matrix precursors and chondrule precursors through relative settling. Astrophys. J. 826, 151. http://dx.doi.org/10.3847/0004-637X/826/2/151.

Johnson, B.C., Minton, D.A., Melosh, H.J., Zuber, M.T., 2015. Impact jetting as the origin of chondrules. Nature 517, 339–341. http://dx.doi.org/10.1038/nature14105.

Kita, N.T., Yin, Q.Z., MacPherson, G.J., Ushikubo, T., Jacobsen, B., Nagashima, K., Kurahashi, E., Krot, A.N., Jacobsen, S.B., 2013. ^{26}Al–^{26}Mg isotope systematics of the first solids in the early solar system. Meteorit. Planet. Sci. 48, 1383–1400. http://dx.doi.org/10.1111/maps.12141.

Krot, A.N., Amelin, Y., Cassen, P., Meibom, A., 2005. Young chondrules in CB chondrites from a giant impact in the early Solar System. Nature 436, 989–992. http://dx.doi.org/10.1038/nature03830.

Krot, A.N., Scott, E.R.D., Zolensky, M.E., 1995. Mineralogical and chemical modification of components in CV3 chondrites: nebular or asteroidal processing? Meteorit. Planet. Sci. 30, 748–775. http://dx.doi.org/10.1111/j.1945-5100.1995.tb01173.x.

Kruijer, T.S., Touboul, M., Fischer-Gödde, M., Bermingham, K.R., Walker, R.J., Kleine, T., 2014. Protracted core formation and rapid accretion of protoplanets. Science 344, 1150–1154. http://dx.doi.org/10.1126/science.1251766.

Meyer, B.S., Clayton, D.D., The, L.S., 2000. Molybdenum and zirconium isotopes from a supernova neutron burst. Astrophys. J. 540, L49–L52. http://dx.doi.org/10.1086/312865.

Nicolussi, G.K., Pellin, M.J., Lewis, R.S., Davis, A.M., Amari, S., Clayton, R.N., 1998. Molybdenum isotopic composition of individual presolar silicon carbide grains from the Murchison meteorite. Geochim. Cosmochim. Acta 62, 1093–1104. http://dx.doi.org/10.1016/S0016-7037(98)00038-6.

Nittler, L.R., Amari, S., Zinner, E., Woosley, S.E., Lewis, R.S., 1996. Extinct ^{44}Ti in presolar graphite and SiC: proof of a supernova origin. Astrophys. J. 462, L31–L34. http://dx.doi.org/10.1088/1538-4357/462/1/L31.

Palme, H., Hezel, D.C., Ebel, D.S., 2015. The origin of chondrules: constraints from matrix composition and matrix-chondrule complementarity. Earth Planet. Sci. Lett. 411, 11–19. http://dx.doi.org/10.1016/j.epsl.2014.11.033.

Palme, H., Lodders, K., Jones, A., 2014a. Solar System abundances of the elements. In: Holland, H.D., Turekian, K.K. (Eds.), Treatise on Geochemistry, second edition. Elsevier, Oxford, pp. 15–36.

Palme, H., Spettel, B., Hezel, D., 2014b. Siderophile elements in chondrules of CV chondrites. Chem. Erde 74, 507–516. http://dx.doi.org/10.1016/j.chemer.2014.06.003.

Pellin, M.J., Calaway, W.F., Davis, A.M., Lewis, R.S., Amari, S., Clayton, R.N., 2000. Toward complete isotopic analysis of individual presolar silicon carbide grains: C, N, Si, Sr, Zr, Mo, and Ba in single grains of type X. Lunar Planet. Sci. Conf. #1917.

Prombo, C.A., Podosek, F.A., Amari, S., Lewis, R.S., 1993. s-process Ba isotopic compositions in presolar SiC from the Murchison meteorite. Astrophys. J. 410, 393–399. http://dx.doi.org/10.1086/172756.

Qin, L., Nittler, L.R., Alexander, C.M.O'D., Wang, J, Stadermann, F.J., Carlson, R.W., 2011. Extreme ^{54}Cr-rich nano-oxides in the CI chondrite Orgueil – implication for a late supernova injection into the solar system. Geochim. Cosmochim. Acta 75, 629–644. http://dx.doi.org/10.1016/j.gca.2010.10.017.

Regelous, M., Elliott, T., Coath, C.D., 2008. Nickel isotope heterogeneity in the early Solar System. Earth Planet. Sci. Lett. 272, 330–338. http://dx.doi.org/10.1016/j.epsl.2008.05.001.

Sanders, I.S., 1996. A chondrule-forming scenario involving molten planetesimals. In: Hewins, R.H., Jones, R.H., Scott, E.R.D. (Eds.), Chondrules and the Protoplanetary Disk. Cambridge University Press, Cambridge, pp. 327–334.

Sanders, I.S., Scott, E.R.D., 2012. The origin of chondrules and chondrites: debris from low-velocity impacts between molten planetesimals? Meteorit. Planet. Sci. 47, 2170–2192. http://dx.doi.org/10.1111/maps.12002.

Shukolyukov, A., Lugmair, G.W., 2006. Manganese–chromium isotope systematics of carbonaceous chondrites. Earth Planet. Sci. Lett. 250, 200–213. http://dx.doi.org/10.1016/j.epsl.2006.07.036.

Trinquier, A., Birck, J.L., Allègre, C.J., 2007. Widespread ^{54}Cr heterogeneity in the inner Solar System. Astrophys. J. 655, 1179–1185. http://dx.doi.org/10.1086/510360.

Walsh, K.J., Morbidelli, A., Raymond, S.N., O'Brien, D.P., Mandell, A.M., 2011. A low mass for Mars from Jupiter's early gas-driven migration. Nature 475, 206–209. http://dx.doi.org/10.1038/nature10201.

Warren, P.H., 2011. Stable-isotopic anomalies and the accretionary assemblage of the Earth and Mars: a subordinate role for carbonaceous chondrites. Earth Planet. Sci. Lett. 311, 93–100. http://dx.doi.org/10.1016/j.epsl.2011.08.047.

Wasson, J.T., 2000. Oxygen-isotopic evolution of the solar nebula. Rev. Geophys. 38, 491–512. http://dx.doi.org/10.1029/2000RG000083.

Wood, J.A., 2005. The chondrite types and their origins. In: Krot, A.N., Scott, E.R.D., Reipurth, B. (Eds.), Chondrites and the Protoplanetary Disk. Astronomical Society of the Pacific, San Francisco, pp. 953–971.

Yokoyama, T., Alexander, C.M.O'D., Walker, R.J., 2011. Assessment of nebular versus parent body processes on presolar components present in chondrites: evidence from osmium isotopes. Earth Planet. Sci. Lett. 305, 115–123. http://dx.doi.org/10.1016/j.epsl.2011.02.046.

Yokoyama, T., Rai, V.K., Alexander, C.M.O'D., Lewis, R.S., Carlson, R.W., Shirey, S.B., Thiemens, M.H., Walker, R.J., 2007. Osmium isotope evidence for uniform distribution of *s*- and *r*-process components in the early solar system. Earth Planet. Sci. Lett. 259, 567–580. http://dx.doi.org/10.1016/j.epsl.2007.05.017.

Zinner, E., Amari, S., Lewis, R.S., 1991. s-Process Ba, Nd, and Sm in presolar SiC from the Murchison meteorite. Astrophys. J. 382, L47–L50. http://dx.doi.org/10.1086/186210.

Zook, H.A., 1981. On a new model for the generation of chondrites. Lunar Planet. Sci. Conf., 1242–1244.